Structural and electronic properties of pyrope garnet ($Mg_3Al_2Si_3O_{12}$): an *ab initio* study

1996 J. Phys.: Condens. Matter 8 8815

(http://iopscience.iop.org/0953-8984/8/45/016)

J. Phys.: Condens. Matter **8** (1996) 8815–8828. Printed in the UK

Structural and electronic properties of pyrope garnet ($Mg_3Al_2Si_3O_{12}$): an *ab initio* study

Ph D'Arco†, F Freyria Fava‡, R Dovesi‡ and V R Saunders§

† Laboratoire de Géologie, Ecole Normale Supérieure, 24 rue Lhomond, 75005 Paris, France

‡ Department of Inorganic, Physical and Materials Chemistry, University of Torino, via P Giuria 5, I-10125 Torino, Italy

§ Daresbury Laboratory, Science and Engineering Council, Daresbury, Cheshire WA4 4AD, UK

Received 31 July 1996

Abstract. The structural and electronic properties of the pyrope garnet have been investigated with the periodic *ab initio* quantum mechanical program CRYSTAL. An all-electron extended basis set of gaussian-type functions has been used. The geometrical parameters of the unit cell, which contains 80 atoms, have been fully optimized. The calculated static geometry agrees with experiment. The bulk modulus and the enthalpy of formation from atoms (binding energy) and simple oxides (MgO, Al_2O_3, SiO_2-quartz) are also evaluated and turn out to be in good agreement with experimental results. Densities of states, charge-density maps and Mulliken population data are used for discussing the electronic structure and nature of the different bonds of the system.

1. Introduction

Natural garnets form a widespread group of silicates closely related by their structural, chemical, and physical properties. For this reason, they have been extensively studied by petrologists and mineralogists. A large number of synthetic garnet crystals have found applications in many fields [1]. Garnets show interesting magnetic properties; some of them (for example andradite ($Ca_3Fe_2Si_3O_{12}$) and almandine ($Al_2Fe_3Si_3O_{12}$)) are antiferromagnetic [2]; others (for example $Y_3Fe_2Fe_3O_{12}$) are ferrimagnetic. Their spin-glass state has been the object of numerous investigations [3]. The technological use of garnets ranges from lasers [4] to computer memories, to many devices where they are used as microwave optical elements [5, 6].

All of these interesting features of garnets are related to their chemistry and their structure. The first structural determination of a garnet (grossular ($Ca_3Al_2Si_3O_{12}$)) is due to Menzer in 1926 [7], who, two years later [8], showed that the other natural garnets are isostructural with grossular. Garnets are cubic with space group $Ia3d$, and their structural formula is $X_3Y_2Z_3O_{12}$. The structure is sketched in figure 1. Atom Z (silicon in the present case) is fourfold coordinated, and located at a 24d site with $\bar{4}$ symmetry. Y cations (Al), located at 16a sites with $\bar{3}$ symmetry, are at the centre of irregular oxygen octahedra. The X cations (Mg) sitting on 24c sites are eightfold coordinated in an oxygen triangular dodecahedron. Oxygen is located at a general position (x, y, z), and is formally bonded to four cations: one Z, one Y and two X. This results in a high percentage of edges being shared between the SiO_4, AlO_6 and MgO_8 polyhedra, that, as a consequence of the general position of oxygen, turn out to be irregular (see table 4, later); the four Si–O and six Al–O

0953-8984/96/458815+14$19.50

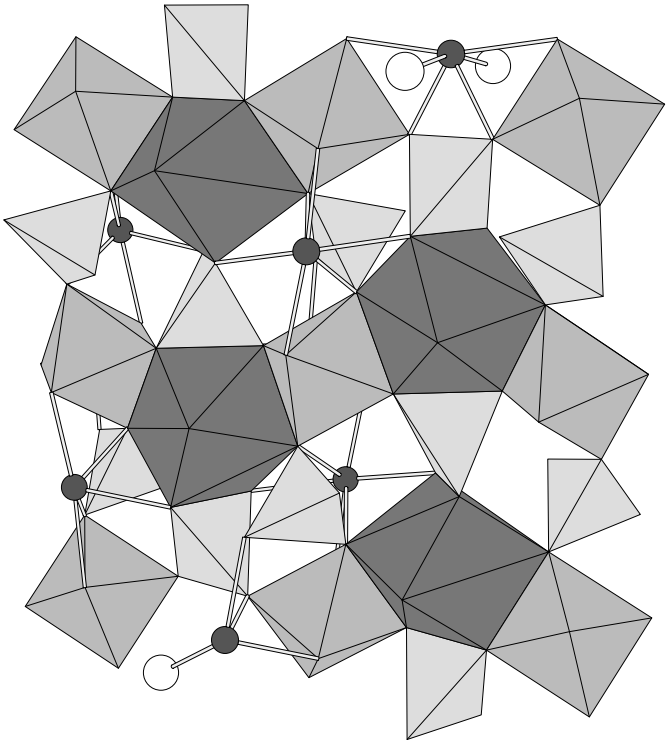

Figure 1. A sketch of the garnet structure. Tetrahedra, octahedra and triangular dodecahedra are occupied by Si, Al, and Mg, respectively. Oxygens at the polyhedra vertices are not represented. Solid and open circles are Mg and O ions, respectively, belonging to not completely represented polyhedra. They are plotted in order to illustrate the fourfold coordination of oxygen.

distances are however equal, whereas the eight Mg–O distances in the dodecahedra split into two sets.

As regards theoretical investigations, the very few studies available in the literature refer to electrostatic or model potential schemes. On the basis of such a model, Born and Zemann [9] concluded that the garnet structure is unstable if the X cation is larger than the Ca ion or smaller than the Mg ion. In fact, the large heat capacity of pyrope at low temperature and its excess heat capacity in solid solutions have been interpreted as consequences of the unusually large MgO_8 polyhedron [10]. In such a large site, Mg could in principle occupy several positions. The numerous pyrope structure refinements however prevent us from confirming this interpretation. More recently, Winkler *et al* [11] performed static lattice energy minimization and lattice dynamics calculations using model potentials including two-body interactions (Buckingham and Born–Mayer-type potentials), three-body bond-bending interactions and a core shell model for O ions [12]. The Coulomb interaction was evaluated using formal charges. The results were in reasonable agreement with experiment; in particular, the cell parameters of grossular and pyrope were underestimated by 0.28 and 0.15 Å, respectively.

To our knowledge, no *ab initio* study of silicate garnets has been published yet, the reason for this being the large unit cell size (80 atoms per cell), only partially counterbalanced by the high degree of point symmetry ($m\bar{3}m$ with 48 symmetry operators).

One of the goals of this paper is to show that, thanks to recent improvements in the quantum mechanical code CRYSTAL [13] and computer performance, it is now possible to tackle the investigation of large systems of primary interest in geophysics and materials science at a more sophisticated level than in the past, that is by using an *ab initio* approach, with an extended *all-electron* variational basis set. As a first step in the direction of a systematic study of such an important class of materials as garnets, the electronic and structural properties of pyrope ($Mg_3Al_2Si_3O_{12}$) have been investigated. Pyrope is one of the most important silicate end-members of the family; it is constituted by light elements, so the calculation is less expensive than when transition metal atoms are involved.

The paper is organized as follows. The computational details are presented in section 2. In section 3 results are presented, concerning the equilibrium geometry and the bulk modulus (section 3.1), the energy of formation from atoms and simple oxides (section 3.2), and the electronic structure described in terms of charge-density maps, Mulliken analysis and densities of states (section 3.3).

2. Computational details

The calculations have been performed within the periodic Hartree–Fock (HF) crystalline orbitals (LCAO) self-consistent scheme as implemented in the CRYSTAL program [13]. Bloch functions are built from local functions ('atomic orbitals' (AOs)) which are linear combinations ('contractions') of gaussian-type functions; the latter are products of gaussians with real solid spherical harmonics Y_l^m; in short, these functions are indicated as s, p, and d AOs when $l = 0$, 1, 2, respectively. The basis sets used for the four atoms in bulk calculations are given in table 1; 13 AOs (4s and 9p) are used for oxygen and magnesium, resulting from 8–4–1–1G (O) and 8–5–1–1G (Mg) contractions; the second, third and fourth contractions refer to shells containing s and p functions sharing the exponents (this constraint being introduced for computational efficiency); the first contraction refers to s functions. For Al and Si, 18 AOs are used (4s, 9p and 5d), resulting from 8–5–1–1G* (the star indicates the presence of d polarization functions) and 8–6–3–1G* contractions, respectively. The basis set has been implemented in previous studies on MgO, Al_2O_3 and SiO_2 [14, 15]. The exponent of the most diffuse valence sp shell of each atom has however been optimized in bulk pyrope for the experimental geometry [16]. The energy gain resulting from this optimization is small (about 7 mHartree per formula unit). For the evaluation of the energy of formation from neutral atoms, the oxygen basis set of table 1 must be reoptimized in order to take into account the tails of the atomic wave functions in the isolated atoms. For Mg, Al and Si, additional diffuse functions have also been included (2, 2 and 1 for Mg, Al and Si, respectively) for a better description of the 3s and p electrons. In this way a basis set of roughly the same variational efficiency has been used for the bulk and the isolated atoms. The resulting atomic energies are reported in table 5, later.

For computational reasons (we recall that this is the first *ab initio* calculation on a garnet), d functions were used only for Si and Al during the geometry optimization. However, single-energy-point calculations have been performed with richer basis sets containing d functions also for Mg and for Mg and O. The importance of d polarization functions is documented in table 2. The energy gain resulting from the subsequent addition of a d shell is at its maximum for Si (90 mHartree per Si atom), and at its minimum for Mg and O (5 and 6 mHartree per atom, respectively), as expected from general consideration (empty d levels are closer to valence levels in Si than in Al and Mg; Si is fourfold coordinated and is involved in quite covalent bonds, whereas Mg is fully ionic and has essentially no valence electrons; Al is in between). As regards atomic charges, d orbitals permit a better redistribution of

Table 1. Basis sets adopted in the present study for bulk calculations. Exponents are in Bohr^{-2} and contraction coefficients multiply individually normalized gaussians.

	Oxygen			Magnesium		
Functions	Exponents	Coefficients s	Coefficients p	Exponents	Coefficients s	Coefficients p
s	$8.020\,00 \times 10^{3}$	1.0800×10^{-3}		$6.837\,19 \times 10^{4}$	2.2260×10^{-4}	
	$1.338\,00 \times 10^{3}$	8.0400×10^{-3}		$9.699\,34 \times 10^{3}$	1.8982×10^{-3}	
	$2.554\,00 \times 10^{2}$	5.3240×10^{-2}		$2.041\,18 \times 10^{3}$	1.1045×10^{-2}	
	$6.922\,00 \times 10^{1}$	1.6810×10^{-1}		$5.298\,63 \times 10^{2}$	5.0063×10^{-2}	
	$2.390\,00 \times 10^{1}$	3.5810×10^{-1}		$1.591\,86 \times 10^{2}$	1.6912×10^{-1}	
	9.264 00	3.8550×10^{-1}		$5.468\,48 \times 10^{1}$	3.6703×10^{-1}	
	3.851 00	1.4680×10^{-1}		$2.123\,57 \times 10^{1}$	4.0041×10^{-1}	
	1.212 00	7.2800×10^{-2}		8.746 04	1.4987×10^{-1}	
sp	$4.943\,00 \times 10^{1}$	-8.8300×10^{-3}	9.5800×10^{-3}	$1.567\,95 \times 10^{2}$	-6.2400×10^{-3}	7.7200×10^{-3}
	$1.047\,00 \times 10^{1}$	-9.1500×10^{-2}	6.9600×10^{-2}	$3.103\,39 \times 10^{1}$	-7.8820×10^{-2}	6.4270×10^{-2}
	3.235 00	-4.0200×10^{-2}	2.0650×10^{-1}	9.645 30	-7.9920×10^{-2}	2.1040×10^{-1}
	1.217 00	3.7900×10^{-1}	3.4700×10^{-1}	3.710 90	2.9063×10^{-1}	3.4314×10^{-1}
				1.611 64	5.7164×10^{-1}	3.7350×10^{-1}
sp	$5.000\,00 \times 10^{-1}$	1.0000	1.0000	$6.800\,00 \times 10^{-1}$	1.0000	1.0000
sp	$2.210\,00 \times 10^{-1}$	1.0000	1.0000	$2.800\,00 \times 10^{-1}$	1.0000	1.0000

	Aluminium			Silicon		
Functions	Exponents	Coefficients s	Coefficients p or d	Exponents	Coefficients s	Coefficients p or d
s	$7.051\,00 \times 10^{4}$	2.2260×10^{-4}		$8.764\,58 \times 10^{4}$	2.3700×10^{-4}	
	$1.008\,00 \times 10^{4}$	1.9000×10^{-3}		$1.285\,18 \times 10^{4}$	1.9200×10^{-3}	
	$2.131\,00 \times 10^{3}$	1.1100×10^{-2}		$2.786\,28 \times 10^{3}$	1.0900×10^{-2}	
	$5.475\,00 \times 10^{2}$	5.0900×10^{-2}		$7.280\,43 \times 10^{2}$	4.9600×10^{-2}	
	$1.631\,00 \times 10^{2}$	1.6970×10^{-1}		$2.195\,16 \times 10^{2}$	1.6680×10^{-1}	
	$5.448\,00 \times 10^{1}$	3.6880×10^{-1}		$7.590\,06 \times 10^{1}$	3.6300×10^{-1}	
	$1.905\,00 \times 10^{1}$	3.5460×10^{-1}		$2.946\,02 \times 10^{1}$	0.4051×10^{-1}	
	5.402 00	4.4300×10^{-2}		$1.198\,91 \times 10^{1}$	0.1504×10^{-1}	
sp	$1.396\,00 \times 10^{2}$	-1.1200×10^{-2}	8.9000×10^{-3}	$1.659\,58 \times 10^{2}$	-8.8400×10^{-3}	9.0900×10^{-3}
	$3.253\,00 \times 10^{1}$	-1.1360×10^{-1}	6.0600×10^{-2}	$3.937\,27 \times 10^{1}$	-8.5900×10^{-2}	6.0100×10^{-1}
	$1.023\,00 \times 10^{1}$	-7.1100×10^{-2}	1.9740×10^{-1}	$1.271\,12 \times 10^{1}$	-7.1200×10^{-1}	1.9520×10^{-1}
	3.810 00	5.2690×10^{-1}	3.1860×10^{-1}	4.717 70	4.1470×10^{-2}	3.3840×10^{-1}
	1.517 00	7.6750×10^{-1}	2.9950×10^{-1}	1.8482	6.1680×10^{-1}	3.0060×10^{-1}
				0.7365	1.1540×10^{-1}	6.4800×10^{-2}
sp	$5.900\,00 \times 10^{-1}$	1.0000	1.0000	4.1752	-1.9900×10^{-2}	-8.7000×10^{-3}
				1.4472	-1.8640×10^{-1}	-4.3800×10^{-3}
				5.023×10^{-1}	9.67×10^{-2}	2.2070×10^{-1}
sp	$2.800\,00 \times 10^{-1}$	1.0000	1.0000	$1.970\,00 \times 10^{-1}$	1.0000	1.0000
d	$6.000\,00 \times 10^{-1}$		1.0000	$6.000\,00 \times 10^{-1}$		1.0000

Table 2. The effect of d polarization functions on the total energy and charges. Q and q_d stand for the net charge and the population of the d shell respectively. Charges were evaluated according to a Mulliken partition scheme. ΔE is the energy reduction per mole due to the addition of the d shell on the indicated atom.

		Adopted basis sets								
Atom	Charges	No d	+	d_{Si}	+	d_{Al}	+	d_{Mg}	+	d_O
Si	Q	2.254		1.842		1.796		1.777		2.231
	q_d			0.335		0.336		0.337		0.291
Al	Q	2.437		2.393		2.276		2.269		2.323
	q_d					0.135		0.135		0.134
Mg	Q	1.854		1.832		1.818		1.796		1.786
	q_d							0.021		0.029
O	Q	−1.433		−1.317		−1.283		−1.271		−1.391
	q_d									0.013
	ΔE	—		−0.2710		−0.0537		−0.0140		−0.0725

valence electrons between each cation and the surrounding anions in the three polyhedra SiO_4, AlO_6 and MgO_8. Adding d functions on Si has a major effect in terms of charge transfer (about $0.4|e|$); for Al this effect is much smaller ($0.12|e|$) and it is even less for magnesium ($0.02|e|$); the charge transfers are in line with the corresponding energy gains.

As regards the computational conditions for the evaluation of the Coulomb and exchange series, the truncation tolerances defined by such as [17, 13] are 6, 6, 6, 6, and 12. The integration in reciprocal space has been performed taking into account only three k-points in the irreducible Brillouin zone (IBZ), resulting from the use of a shrinking factor (IS) equal to 2: (0, 0, 0), (1, 0, 0), and (1, 1, 1) in units of $b/2$ where b is the reciprocal basis vector. The use of such a small IS value is justified by the large size of the cell; the energy difference with respect to a calculation performed with a denser net of k-points (eight k-points in the IBZ obtained with IS = 4) is less than 1×10^{-5} hartrees per cell.

The main limitation of the present scheme is related to the so-called correlation error, that is the lack of instantaneous correlation of the motion of electrons (the HF method is based on a mean-field scheme). This limitation has been shown to have only a minor influence on the calculated geometry (and, to lesser extent, also on the elastic properties) of ionic compounds containing light atoms, such as Al_2O_3, MgO, $MgAl_2O_4$ [15] and $MgSiO_3$ [18]. The error for the linear geometrical parameters of these compounds is less than 1%; the elastic properties are overestimated by 7 to 15%. The error is larger for energies of formation from atoms or simple oxides, in particular if there is a large density difference between complex compounds and simple oxides. Typically, the binding energy can be underestimated at the HF level by 30 to 50% [19, 20]. For the above properties, an estimate of the correlation energy is performed [19] by using a correlation-only gradient-corrected density functional [21] scheme. The correlation energy is obtained as the integral over the unit cell of a function [21] of the crystalline Hartree–Fock charge density. This *a posteriori* correction is very effective in reducing the error in binding energy (BE) and relative stability of different phases evaluated at the HF level to few per cent [18, 19, 22]. In the following, this scheme will be applied in the evaluation of the BE (the energy of formation from atoms) and the energy of formation of pyrope from simple oxides.

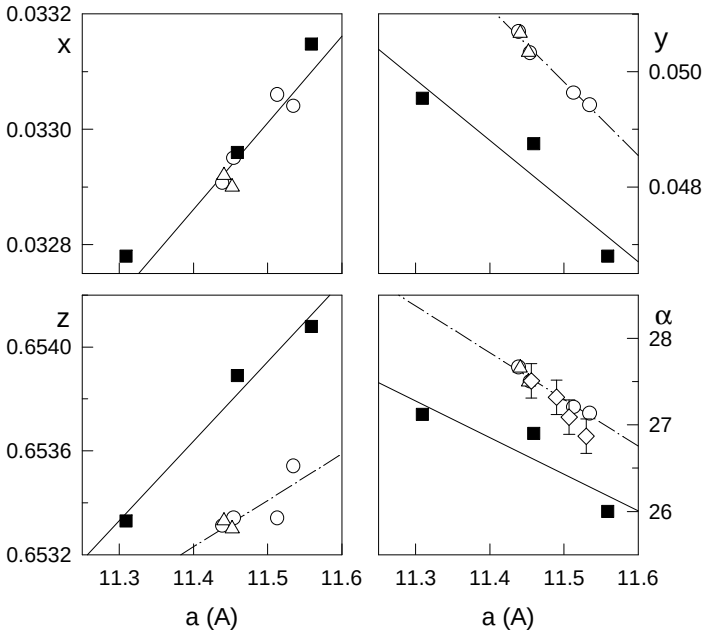

Figure 2. Variations of the fractional coordinates of oxygen (x, y, z) and of the rotation angle of the tetrahedron (α in degrees) as functions of the cell parameter. Solid and open symbols refer to calculated and experimental values, respectively. Circles, triangles, and diamonds correspond to data from references [24], [23] and [25], respectively. For the latter data, the error bar quoted by the author is plotted. Solid and chain lines are obtained from a best fit of the present calculated data and the experimental data of Pavese *et al* [24], respectively.

Table 3. The calculated and experimental structure and bulk modulus of pyrope. a is the lattice parameter (in Å), x, y, z are the oxygen fractional coordinates, and B is the bulk modulus in GPa. The ranges of experimental values for isothermal (^{T}) and adiabatic (^{S}) bulk moduli are from [38–40] and [41–45], respectively.

	Calculated		
	This study	Winkler *et al* (1991)[a]	Experimental
a	11.459	11.302	11.439[b]
x	0.032 96	0.0311	0.032 91[b]
y	0.048 75	0.0549	0.050 69[b]
z	0.653 89	0.6526	0.653 31 [b]
B	210	202	$(170–179)^T$ $(172–177)^S$

[a] Geometry optimized with a model potential.
[b] Experimental structure from reference [24] refined at 30 K.

3. Results and discussion

3.1. The structure

The calculated equilibrium geometry and bulk modulus are reported in table 3. The equilibrium geometry has been obtained as follows: for three lattice parameters (a =

11.309, 11.459 and 11.559 Å) the oxygen fractional coordinates have been numerically optimized according to a conjugate gradient scheme. The equilibrium value of each coordinate was obtained by fitting three energy points. Only two optimization cycles could be performed due to computational cost. Figure 2 shows that the three calculated oxygen fractional coordinates vary almost linearly with the lattice parameter. The slightly erratic behaviour can be attributed to the roughness of the numerical minimization process. The bottom right-hand plot in figure 2 shows the variation of α, the rotation angle of the tetrahedron about the $\bar{4}$ axis, as first defined by Born and Zemann [9]. α is given by $\alpha = \tan^{-1}(y/(0.75 - z))$, and is therefore extremely sensitive to small errors in y and z.

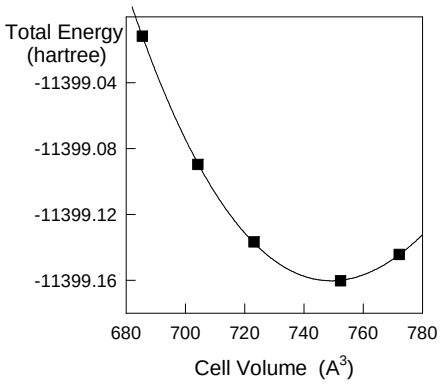

Figure 3. The total energy as a function of the cell volume.

In figure 2, the experimental results from Ambruster *et al* [23], Pavese *et al* [24], and Meagher [25] are also reported, which however refer to the effect of *temperature* on the pyrope structure. In spite of the fact that the calculated and experimental data are not perfectly homogeneous, trends are very similar for the four variables considered. This point calls for some remarks. Hazen and Prewitt [26] have noted that the pressure-induced structural changes on loading are similar to those due to cooling in several silicate groups. Hazen and Finger [27] in their structural study of pyrope up to a pressure of 5.9 GPa indicated that pyrope also displays this relationship. Unfortunately, their data do not show any monotonic variation of the oxygen coordinates as a function of pressure. However, as the volume range defined by our three fully optimized structures covers that studied by these authors, we can compare our and their linear bond compressibility (χ) ratios [27]. The calculated values are as follows: $\chi_{SiO}/\chi_{AlO} = 0.43$, $\chi_{SiO}/\chi_{MgO} = 0.33$, $\chi_{AlO}/\chi_{MgO} = 0.77$ in fairly good agreement with those derived from bond compressibility quoted by Hazen and Finger [27]: $\chi_{SiO}/\chi_{AlO} = 0.58$, $\chi_{SiO}/\chi_{MgO} = 0.41$, and $\chi_{AlO}/\chi_{MgO} = 0.70$.

It is interesting to note that similar variations of the x- and y-coordinates of oxygen as functions of the cell parameter can be obtained for garnets where Ca, Fe, and Mn substitute for Mg [16, 23]. However, the corresponding variation of z is inverse to that reported here.

In order to evaluate the bulk modulus, two additional volumes were considered (a = 11.109 and 11.209 Å); the corresponding oxygen position was obtained from the $x(a)$, $y(a)$, and $z(a)$ straight lines in figure 2. The calculated E versus V energy points are plotted in figure 3 together with the interpolating third-order polynomial. The equilibrium cell parameter of the static lattice at zero pressure is 11.446 Å which compares fairly well with the low-temperature measurement (11.439 Å at 30 K, as measured by Pavese *et al* [24]), or with the classical athermal limit obtained from high-temperature data (11.428 Å).

As the minimum-energy cell parameter is extremely close (0.1%) to the fully optimized point at 11.459 Å, we will refer to the latter one as the optimized structure. In table 3, the equilibrium geometry obtained by Winkler *et al* [11] is also reported for comparison.

Table 4. Calculated and experimental distances (Å) and corresponding calculated bond populations (in 10^{-3} electron unit), and internal angles in polyhedra (deg). The oxygens' superscripts correspond to the Novak and Gibbs labelling [16]. The subscripts and superscripts (d, t, o) indicate the two polyhedra to which the O–O edge belongs; when only one label is given, the two oxygen atoms belong to the same polyhedron. *N* indicates the multiplicity for one polyhedron. The experimental data were obtained at 30 K [24].

		N	Calculated	Experiment	Bond population
X–O	Si–O	4	1.624	1.634	302
	Al–O	6	1.888	1.885	87
	$Mg–O^1$	4	2.191	2.196	18
	$Mg–O^4$	4	2.360	2.333	11
O–O	$(O^1–O^2)^t_d$	2	2.470	2.498	−70
	$(O^1–O^4)^o_d$	6	2.629	2.613	−19
	$(O^5–O^4)_o$	6	2.710	2.717	−16
	$(O^4–O^6)^d_d$	4	2.726	2.699	−19
	$(O^1–O^3)_t$	4	2.739	2.749	−28
	$(O^4–O^7)_d$	2	2.806	2.769	−9
O–X̂–O	O^1–Si–O^2	2	99.00	99.70	
	O^1–Si–O^3	4	114.94	114.57	
	O^1–Al–O^4	6	88.26	87.77	
	O^1–Al–O^5	6	91.73	92.23	

The agreement between our calculated and experimental bond lengths and angles is fairly good, as shown in table 4. The largest bond length discrepancies refer to the SiO and MgO bonds with relative errors of −0.6% and +1.2% respectively. The oxygen–oxygen distances, which correspond to second neighbours, are accurately reproduced. Only the O_5–O_4 and O_4–O_6 distances are inverted; however, they differ by only 0.018 Å in the experimental geometry. The angular distortion of the SiO_4 tetrahedron and AlO_6 octahedron is correctly mimicked. The largest difference between calculated and experimental O–Si–O and O–Al–O angles is 0.7°.

Table 5. Calculated and experimental binding energies (BE) of pyrope. E_{HF} and E_{HF+C} are the total energies evaluated at the Hartree–Fock level and after inclusion of the correlation energy E_C. The H_{ath} are the experimental enthalpies of formation from elements in their reference state reduced to the athermal limit. Units: hartrees per mole.

		O	Mg	Al	Si	$Mg_3Al_2Si_3O_{12}$	BE
Calculated	E_{HF}	−74.8012	−199.6042	−241.8670	−288.8410	−2849.7903	−3.1063
	E_C	−0.2661	−0.4479	−0.4871	−0.5290	−7.9715	−0.8738
	E_{HF+C}	−75.0673	−200.0521	−242.3541	−289.3700	−2857.7618	−3.9797
Experiment	H_{ath}	0.0949	0.0560	0.1257	0.1714	−2.4110	−4.4834

The bulk modulus (B) estimated via a third-order polynomial fit to the $E(V)$ curve (figure 3) is equal to 210 GPa; it reduces to 205 GPa when a Birch–Murnaghan equation of

Table 6. Formation energies (ΔE) of pyrope from simple oxides. The notation is as in table 5. H_{298} is the standard enthalpy of formation from oxides, $H_0 - H_{298}$ and E_{zp} are the corrections for the temperature effect and zero-point motion; H_{ath} is the resulting athermal enthalpy. Energies are in hartrees per mole.

		MgO	Al_2O_3	SiO_2	$Mg_3Al_2Si_3O_{12}$	ΔE
Calculation	E_{HF}	−274.6734	−708.9792	−438.9289	−2849.7903	−0.0042
	E_C	−0.7901	−2.0076	−1.1921	−7.9715	−0.0173
	E_{HF+C}	−275.4635	−710.9868	−440.1210	−2857.7618	−0.0215
Experiment	H_{298}	0.	0.	0.	−0.0276	−0.0276
	$H_0 - H_{298}$	−0.0020	−0.0038	−0.0026	−0.0182	−0.0006
	E_{zp}	−0.0067	−0.0183	−0.0061	−0.0531	0.0036
	H_{ath}	−0.0087	−0.0221	−0.0087	−0.0989	−0.0246

state is used while the pressure derivative of B (B') is kept constant and equal to 4; if B' is used as a parameter in the fitting procedure, B is equal to 207 GPa ($B' = 3.80$). As shown in table 3, there have been many experimental determinations of B at room temperature, giving values ranging from 170 to 179 GPa. Using the temperature derivative reported by Bonczar *et al* [28] and Sumino and Anderson [29], the bulk modulus at 0 K can be estimated as being between 180 and 183 GPa. Thus, the calculated value of B is larger than the experimental one by about 16%, in line with previous Hartree–Fock calculations. Part of the error is to be attributed to the incomplete geometry optimization of the $E(V)$ energy points used for the fitting, and to basis set incompleteness.

3.2. Binding energy and the enthalpy of formation

All of the data required to estimate the binding energy and the athermal formation enthalpy of pyrope are quoted in tables 5 and 6. The enthalpies of formation of pyrope from oxides and elements are from Robie *et al* [30]. They have been reduced to the athermal limit using low-temperature heat capacity measurements for MgO [31], Al_2O_3 [32], SiO_2 [33], and pyrope [10], and estimates of the zero-point energy from the Debye temperature: 946 K for MgO [31], 1026 K for Al_2O_3 [34], 567 K for SiO_2 [35] and 745 K [36] or 794 K [37] for pyrope (the related zero-point energy difference is 3 mHartree). It turns out (see table 5) that the binding energy estimated at the HF level represents about 70% of the experimental one derived from thermochemical data, in line with previous results for semiconductors [19] and ionic compounds [20]. When correlation energy is taken into account through the '*a posteriori*' scheme discussed in a previous section, the calculated binding energy accounts for 85% of the experimental value. The relative errors in the binding energy at the HF level as well as at the HF + correlation level are similar to those obtained for MgO, Al_2O_3 and SiO_2 [20].

The enthalpies of formation from oxides (MgO, Al_2O_3, and SiO_2-quartz) calculated at the HF level (and referring them to the static limit), with the basis set of table 1, represent only 15% of the experimental data (table 6). Thermal variations of the enthalpy between room and zero temperature and zero-point energy effects (estimated from Debye temperatures) do not alter this result. The large discrepancy is related to the volume difference between pyrope and the oxide mixture. Pyrope is a dense phase with a molar volume about 10% smaller than the volume of the chemically equivalent mixture of oxides. For this reason the correlation energy is expected to be larger for pyrope than for the oxide mixture in favour of the denser phase. When correlation is taken into account the calculated

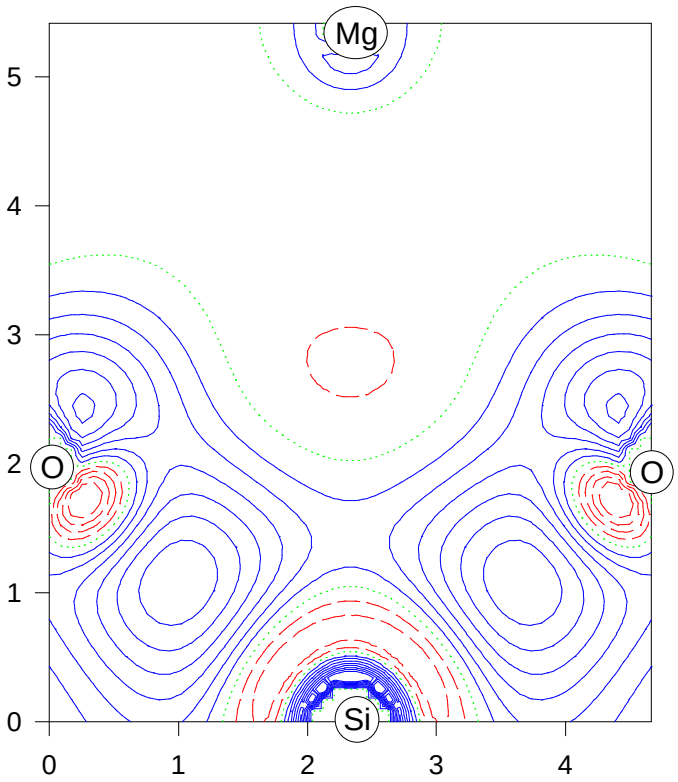

Figure 4. A deformation map. The difference between the bulk charge density and the superposition of ionic (Mg^{2+}, Al^{3+}, Si^{4+}, O^{2-}) spherical charge densities (obtained with the same basis set as was used for the bulk calculation) is reported. The interval between isolines is 0.01 e Bohr^{-3}. Solid, dotted and dashed lines indicate positive, zero, and negative values, respectively. The x- and y-axis scales are in Bohr.

enthalpy of formation dramatically improves to 88% of the experimental result, as shown in table 6.

3.3. Chemical bonding

The Mulliken population data are shown in table 2, where the net atomic charges are reported (the d_{Al} column) and table 4 (the last column), where bond populations are given. The net charge on Mg ($+1.8|e|$) is close to the formal value $+2|e|$, whereas the Al, Si, and O net charges ($+2.4|e|$, $+1.8|e|$, $-1.3|e|$) are significantly different from the formal ionic charges, due to the partial covalent character of the Si–O and Al–O bonds. Bond population (B-) data support this description. We recall that negative values indicate repulsive interactions between ions, while large positive values suggest covalent character of the bond. The smallest cation–oxygen bond populations are the Mg–O ones; their values ($+0.018|e|$ and $+0.011|e|$) are similar to that reported for MgO–B2 [20], where Mg is also eightfold coordinated. B(Si–O) is larger than B(Al–O); both values are very close to those obtained for SiO_2 (α-quartz) and Al_2O_3 (corundum) and indicate medium (Al–O) or strong (Si–O) covalent character of these bonds.

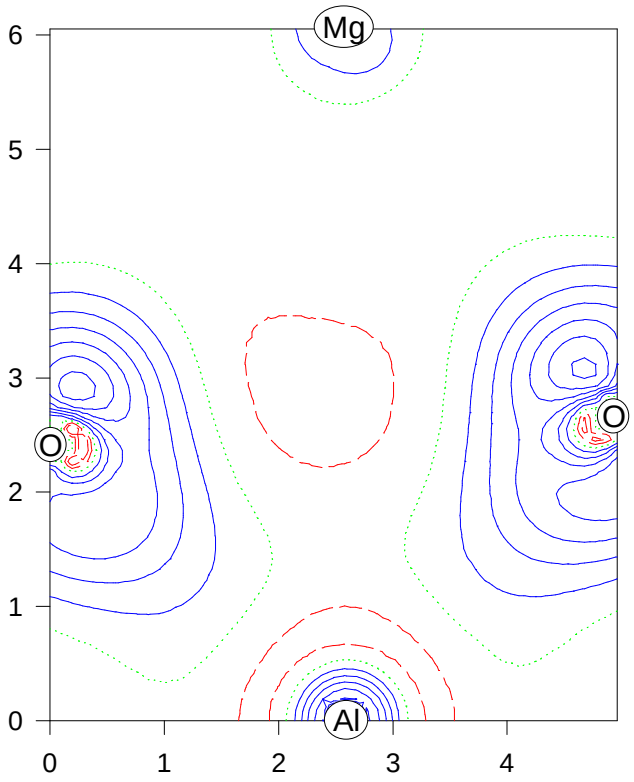

Figure 5. A deformation map. The symbols and scales are as in figure 4.

As indicated by the small, but positive, value of B(Mg–O) and the negative value of $B(O^i–O^j)$, the dominant repulsion within the MgO_8 polyhedra is the O–O one, *not* the Mg–O one. This seems to confirm that the Mg cage is too large for Mg. At the moment, however, we cannot explore the possible positional disorder of Mg in the cage.

The largest negative value of $B(O^i–O^j)$ ($=-0.070$) corresponds to the shortest O–O distance in the structure. These two oxygens define an edge shared by SiO_4 and MgO_8 polyhedra; the corresponding Si–Mg distance is the shortest cation–cation distance in the structure (2.865 Å). The remaining values of B(O–O) decrease as a function of the O–O distance to values more typical of low-pressure phases. B(Si–Mg) is almost zero, and this indicates that there is no direct interaction between the two cations; the shortening of the shared edge efficiently screens the cation–cation repulsion.

The relatively high number of strong O–O repulsions in the pyrope structure is overcompensated by the very large attractive electrostatic energy resulting from the efficient packing of the three type of polyhedron.

Deformation maps obtained as the differences between the crystal charge density and the superposition of spherical ionic charge distributions are shown in figures 4 and 5. From both figures the fully ionic nature of the Mg–O bond is confirmed. As usual, the Mg^{2+} ion slightly contracts when entering into the crystalline environment, as a consequence of the interionic short-range repulsion. In the upper part of both figures the charge-density difference is very small and negative, as a result of this repulsion. At the centre of the

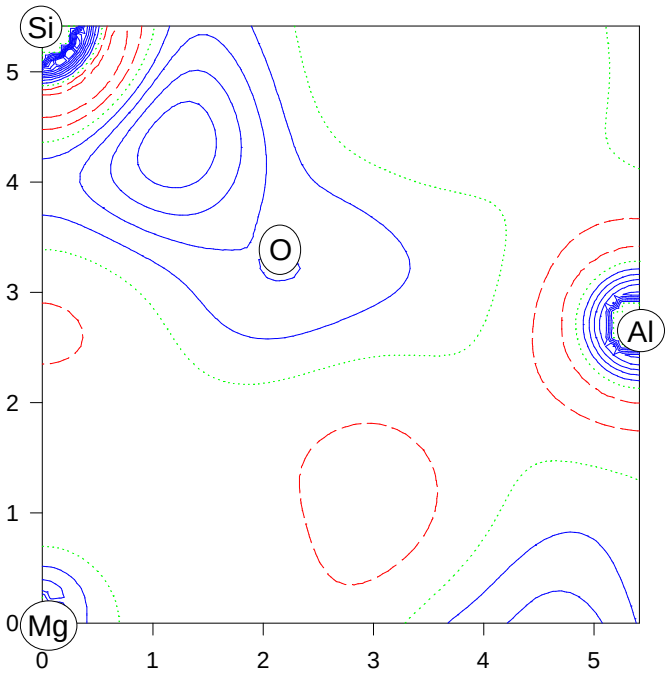

Figure 6. A deformation map. The symbols and scales are as in figure 4. The oxygen lies slightly below the plane of the figure.

figures, along the O–O direction, the function is even more negative because: (a) the isolated oxygen ions (whose charge distribution is subtracted from the bulk one) have a total charge attributed to them that is much larger ($-2|e|$) than the bulk one ($-1.3|e|$); (b) the oxygen charge distribution modifies its spherical shape in order to reduce the O–O repulsion and because partial covalent bonds are formed (with Al and Si) with a resulting charge transfer from the upper to the lower part of the figure. Here the big difference between the two bonds is evident, which confirms the bond population data: in the Si–O case there is a large build-up of charge midway between the two atoms, a typical feature of (strong) covalent bonds; in the Al–O case the oxygen charge distribution is protruding towards Al, but without formation of a real charge plateau midway between the two atoms.

In figure 6, the deformation map in the Si–Mg–Al plane is shown; the oxygen atom sits slightly below the plane of the figure. This figure can be compared to an experimentally derived residual map ([46], figure 1(a)). The two maps show the same main features: a large build-up of charge at about 0.8 Å along the Si–O axis, and a smaller one close to the Mg–Al line. Both maps show an almost zero or negative density in the other regions.

The total and projected density of states plotted in figure 7 shows that pyrope is a highly ionic insulator with a large band gap of about 0.6 Hartree (17 eV).

As usual, the HF band gap is overestimated, the band-gap width determined from spectroscopic data being about 9 eV [47].

The dispersion in the valence band is small (band width: of the order of 0.4 Hartree); the upper part of the valence band is mainly associated with oxygen p states, with minor contributions from Si and Al; the oxygen 2s bands are well separated from the 2p bands. The contribution of cations to conduction bands is larger than that to valence bands.

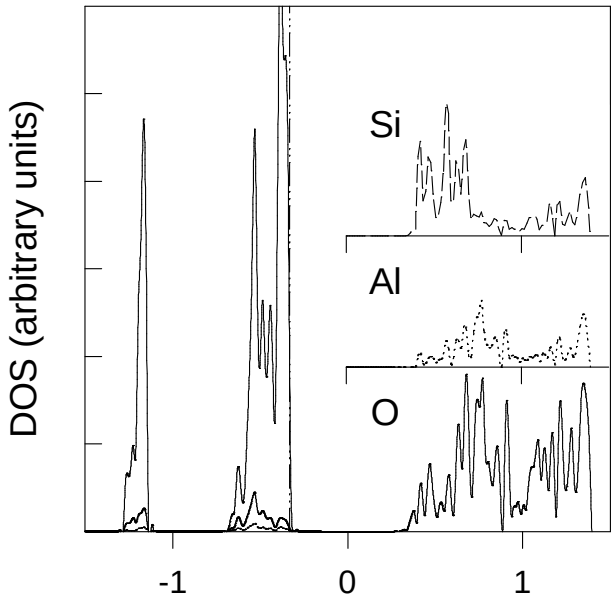

Figure 7. Valence and conduction (positive energy values) projected densities of state (DOS). Dotted, solid and broken lines in the conduction region represent Al, O, and Si contributions, respectively. In the valence DOS, the small Si and Al contributions are also reported.

4. Conclusions

In this paper, it has been shown that the *ab initio* periodic HF technique can now be applied successfully to large-unit-cell systems of utmost importance. Good agreement has been found between the calculated and experimental geometry, bulk modulus and formation energy. The analysis of the charge density and bond population supports the proposal that the dodecahedral cage is not completely filled by Mg. Other garnets are currently under investigation.

Acknowledgments

This work was supported by the Human Capital & Mobility programme of the European Community under contract CHRX-CT93-0155. PD acknowledges the INSU-DBT programme and CNRS for financial support. FFF and RD thank the Italian Ministero dell' Università e della Ricerca Scientifica e Tecnologica (MURST, 60%) and Italian CNR (Consiglio Nazionale delle Ricerche) for financial support.

References

[1] Geller S 1967 *Z. Kristallogr.* **125** 1
[2] Prandl W 1971 *Z. Kristallogr.* **134** 333
[3] Prandl W and Brückel T 1988 *Structural and Magnetic Phase Transitions in Minerals* ed S Ghose, J M D Coey and E Salje (Berlin: Springer) p 208
[4] Struve B and Huber G 1985 *Appl. Phys.* B **36** 195
[5] Bobeck A H, Spencer E G, Van Uitert L G, Abrahams S C, Barns R L, Grodkiewicz W H, Sherwood R C, Schmidt P H, Smith D H and Walters E M 1970 *Appl. Phys. Lett.* **17** 131

[6] Paoletti A (ed) *Physics of Magnetic Garnets ('Enrico Fermi' School of Physics, Course LXX)* (Amsterdam: North-Holland)
[7] Menzer G 1926 *Z. Kristallogr.* **63** 157
[8] Menzer G 1928 *Z. Kristallogr.* **69** 300
[9] Born L and Zemann J 1964 *Beitr. Mineral. Petrog.* **10** 2
[10] Haselton H T and Westrum E F 1980 *Geochim. Cosmochim. Acta* **44** 701
[11] Winkler B, Dove M T and Leslie M 1991 *Am. Mineral.* **76** 313
[12] Catlow C R A 1988 *Physical Properties and Thermodynamic Behaviour of Minerals (NATO ASI series C, vol 225)* ed E Salje (Boston, MA: Reidel) p 619
[13] Dovesi R, Saunders V R and Roetti C 1992 *CRYSTAL 92 User Manual* (Torino: University of Torino)
[14] Causà M, Dovesi R, Pisani C and Roetti C 1986 *Phys. Rev.* B **33** 1308
[15] Catti M, Valerio G, Dovesi R and Causà M 1994 *Phys. Rev.* B **49** 14 179
[16] Novak G A and Gibbs G V 1971 *Am. Mineral.* **56** 791
[17] Pisani C, Dovesi R and Roetti C 1988 *Hartree–Fock ab initio Treatment of Crystalline Systems (Springer Lecture Notes in Chemistry 48)* (Heidelberg: Springer)
[18] D'Arco P, Sandrone G, Dovesi R, Orlando R and Saunders V R 1993 *Phys. Chem. Minerals* **20** 407
[19] Causà M, Dovesi R and Roetti C 1991 *Phys. Rev.* B **43** 11 937
[20] Dovesi R, Roetti C, Freyria Fava C, Aprà E, Saunders V R and Harrison N M 1992 *Phil. Trans. R. Soc.* A **341** 203
[21] Perdew J P 1986 *Phys. Rev.* B **33** 8822 (erratum: 1986 **34** 7406)
Perdew J P, Chevary J A, Vosko S H, Jackson K A, Pederson M R, Singh D J and Fiolhais C 1992 *Phys. Rev.* B **46** 6671
[22] Aprà E, Causà M, Prencipe M, Dovesi R and Saunders V R 1993 *J. Phys.: Condens. Matter* **5** 2969
[23] Ambruster T, Geiger C A and Lager G A 1991 *Am. Mineral.* **77** 512
[24] Pavese A, Artioli G and Prencipe M 1995 *Am. Mineral.* **80** 457
[25] Meagher E P 1975 *Am. Mineral.* **60** 218
[26] Hazen R M and Prewitt C T 1997 *Am. Mineral.* **62** 309
[27] Hazen R M and Finger L W 1978 *Am. Mineral.* **63** 297
[28] Bonczar J L, Graham E K and Wang H 1977 *J. Geophys. Res.* **82** 2529
[29] Sumino Y and Anderson O L 1984 *CRC Handbook of the Physical Properties of Rocks* ed S Carmichael (Boca Raton, FL: Chemical Rubber Company Press) pp 39–138
[30] Robie R A, Hemingway B S and Fischer J R 1979 *US Geol. Survey Bull.* **1452**
[31] Barron T H K, Berg W T and Morrison J A 1959 *Proc. R. Soc.* A **250** 70
[32] Ditmars D A and Douglas T B 1971 *J. Res. NBS* A **75** 401
[33] Richet P, Bottinga Y, Denielou L, Petitet J P and Tequi C 1982 *Geochim. Cosmochim. Acta* **46** 2639
[34] Ginnings D C and Furukawa G T 1953 *J. Am. Chem. Soc.* **75** 522
[35] Lord R C and Morrow J C 1957 *J. Chem. Phys.* **26** 230
[36] Soga N 1967 *J. Geophys. Res.* **72** 4227
[37] Kieffer S W 1980 *Rev. Geophys. Space Phys.* **18** 862
[38] Sato Y, Akaogi M and Akimoto S 1978 *J. Geophys. Res.* **83** 335
[39] Levien L, Prewitt C T and Weidner D J 1978 *EOS Trans. Am. Geophys. Union* **59** 1180
[40] Takahashi T and Liu L G 1970 *J. Geophys. Res.* **75** 5757
[41] Webbs S L 1989 *Phys. Chem. Minerals* **16** 684
[42] Leitner B J, Weidner D J and Liebermann R C 1980 *Phys. Earth Planet. Interiors* **22** 111
[43] Babuska V, Fiala J, Kumazawa M, Ohno I and Sumino Y 1978 *Phys. Earth Planet. Interiors* **16** 157
[44] O'Neill B, Bass J D, Smyth J R and Vaughan M T 1989 *J. Geophys. Res.* **94** 17 819
[45] Wang H and Huang K 1975 *EOS Trans. Am. Geophys. Union* **56** 601
[46] Sawada H 1993 *Z. Kristallogr.* **203** 41
[47] Nitsan U and Shankland T J 1976 *Geophys. J. R. Astron. Soc.* **45** 59